Anal. Chem. **2001,** *73,* 5287−5295

Electrochemical and Quartz Crystal Microbalance Detection of the Cholera Toxin Employing Horseradish Peroxidase And GM1-Functionalized Liposomes

Lital Alfonta and Itamar Willner*

Institute of Chemistry, The Hebrew University of Jerusalem, Jerusalem 91904, Israel

Daniel J. Throckmorton and Anup K. Singh

Chemical and Radiation Detection Laboratories, Sandia National Laboratories, Livermore, California 94550

An ultrasensitive method for the detection of the cholera toxin (CT) using electrochemical or microgravimetric quartz crystal microbalance transduction means is described. Horseradish peroxidase (HRP) and GM1-functionalized liposomes act as catalytic recognition labels for the amplified detection of the cholera toxin based on highly specific recognition of CT by the ganglioside GM1. The sensing interface consists of monoclonal antibody against the B subunit of CT that is linked to protein G, assembled as a monolayer on an Au electrode or an Au/quartz crystal. The CT is detected by a "sandwich-type" assay on the electronic transducers, where the toxin is first bound to the anti-CT-Ab and then to the HRP-GM1-ganglioside-functionalized liposome. The enzyme-labeled liposome mediates the oxidation of 4-chloronaphthol (2) in the presence of H_2O_2 to form the insoluble product 3 on the electrode support or the Au/quartz crystal. The biocatalytic precipitation of 3 provides the amplification route for the detection of the CT. Formation of the insulating film of 3 on the electrode increases the interfacial electron-transfer resistance, R_{et}, or enhances the electrode resistance, R', parameters that are quantitatively derived by Faradaic impedance measurements and chronopotentiometric analyses, respectively. Similarly, the precipitate 3 formed on the Au/quartz crystal results in a mass increase on the transducer that is reflected by a decrease in the resonance frequency of the crystal. The methods allow the detection of the CT with an unprecedented sensitivity that corresponds to 1.0×10^{-13} M.

The assembly of monolayers or multilayers of biomaterials on electronic transducers, e.g., electrodes or piezoelectric crystals, is extensively employed for the development of biosensors.[1,2] Enzyme-layered electrodes,[3,4] antigen (or antibody) layers on electrodes[5] or piezoelectric crystals,[6] and nucleic acid-monolayer-functionalized electrodes[7] were reported as active sensing interfaces for biosensors. A challenging topic in the development of biosensors relates to the sensitivity of the detection methods and to the need to develop amplification schemes for the analyses. Amplified electrochemical detection of antibodies or antigens was accomplished by coupling enzyme-linked bioelectrocatalytic transformations to the antigen−antibody recognition events. Antigens or antibodies were modified with redox enzymes, and the respective antigen or antibody was analyzed by competitive association in the presence of the enzyme-labeled antigen (or antibody) to the sensing interface and by the monitoring of the current resulting from the bioelectrocatalytic transformation.[8] Indirect amplified electrochemical detection of the formation of antibody−antigen complexes was achieved by the coupling of an enzyme to the antigen (or antibody) and the electrochemical detection of a redox-active product generated by the biocatalyst[9,10]

* To whom all correspondence should be addressed. Tel.: 972-2-6585272. Fax: 972-2-6527715. E-mail: willnea@vms.huji.ac.il.

(1) (a) Willner, I.; Katz, E. *Angew. Chem., Int. Ed.* **2000**, *39*, 1180−1218. (b) Willner, I.; Katz, E.; Willner, B. In *Sensors Updates*; Balted, H., Göpel, W., Hesse, J., Eds; Wiley-VCH: Weinheim, Germany, 1999; Vol. 5; pp 45−102.

(2) (a) Göpel, W. *Biosens. Bioelectron.* **1995**, *10*, 35−59. (b) Göpel, W.; Heiduschka, P. *Biosens. Bioelectron.* **1995**, *10*, 853−883. (c) Willner, I.; Katz, E.; Willner, B. *Electroanalysis* **1997**, *9*, 965−977.

(3) (a) Katz, E.; Riklin, A.; Willner, I. *J. Electroanal. Chem.* **1993**, *354*, 129−144. (b) Willner, I.; Riklin, A.; Shoham, B.; Rivenzon, D.; Katz, E. *Adv. Mater.* **1993**, *5*, 912−915.

(4) (a) Willner, I.; Riklin, A. *Anal. Chem.* **1994**, *66*, 1535−1539. (b) Riklin, A.; Willner, I. *Anal. Chem.* **1995**, *67*, 4118−4126. (c) Bourdillon, C.; Demaille, C.; Moiroux, J.; Savéant, J. M. *Acc. Chem. Res.* **1996**, *29*, 529−535.

(5) Blonder, R.; Katz, E.; Cohen, Y.; Itzhak, N.; Riklin, A.; Willner, I. *Anal. Chem.* **1996**, *68*, 3151−3157.

(6) Ben-Dov, I.; Willner, I.; Zisman, E. *Anal. Chem.* **1997**, *69*, 3506−3512.

(7) Patolsky, F.; Lichtenstein, A.; Willner, I. *Angew. Chem., Int. Ed.* **2000**, *39*, 940−943.

(8) (a) Ho, W. O.; Atehy, D.; McNeil, C. J. *Biosens. Bioelectron.* **1995**, *10*, 683−691. (b) Rishpon, J.; Soussan, L.; Rosen-Margalit, I.; Hadas, E. *Immunoassays* **1992**, *13*, 231−235.

(9) (a) Wehmeyer, K. R.; Halsalt, H. B.; Heineman, W. R.; Volle, C. P.; Chen, C. *Anal. Chem.* **1986**, *58*, 135−139. (b) Aizawa, M. In *Electrochemical Sensors in Immunological Analysis*; Ngo, T. T., Ed.; Plenum Press: New York, 1987; pp 269−291.

(10) (a) Uditha de Alwis, W.; Wilson, G. S. *Anal. Chem.* **1985**, *57*, 2754−2756. (b) Ysukouchi, K.; Unoki, M.; Taniguchi, I. *Biosens. Bioelectron.* **1990**, *5*, 87−101. (c) Bier, F. F.; EhrentreichForester, E.; Makower, A.; Scheller, F. W. *Anal. Chim. Acta* **1996**, *328*, 27−32. (d) Bier, F. F.; EhrentreichForester, E.; Scheller, F. W.; Makower, A.; Eremenko, A.; Wollenberger, U.; Bauer, C. G.; Pfeiffer, D.; Michael, N. *Sens. Actuators, B* **1996**, *33*, 5−12.

10.1021/ac010542e CCC: $20.00
Published on Web 09/20/2001

for amperometric or potentiometric detection of NADH, phenol, O_2, H_2O_2, or NH_3 generated by the enzyme-linked antigen (or antibody). The blocking of the electrical contact of redox-tethered enzymes and the electrode, upon formation of the antigen−antibody complex on the conducting support, was used for the development of amperometric immunosensors with amplification features.[5] The biocatalyzed precipitation of an insoluble product on electronic transducers was recently employed as an amplification route for antigen/antibody[11] or DNA detection.[12] The enzyme label that stimulates the biocatalyzed precipitation of the insoluble product on the transducer may be associated to detect biomaterial as an avidin−enzyme conjugate. Electrochemical transduction, e.g., Faradaic impedance spectroscopy or chronopotentiometry, or microgravimetric quartz crystal microbalance measurements, were used as electronic transduction means for the sensing events. Recently, enzyme-functionalized liposomes, e.g., horseradish peroxidase (HRP)-modified liposomes, which included a biotin label, were used as a functional tether for the biocatalyzed precipitation of an insoluble product and the amplification of biomaterial detection.[12c]

Bacterial toxins represent a broad class of molecular and macromolecular materials that cause a variety of human diseases.[13] Toxins secreted by the bacterium *Clostridium botulinum* abolish acetylcholine signaling at the neuromuscular junction and represent a biological warfare threat, enterotoxins produced by *Escherichia coli* or *Salmonella typhimurium* are common food contaminants that cause chronic activation of adenylate cyclase,[14] and aflatoxins produced by the fungal species *Aspergillus flavus* or *Aspergillus parasitieus* appear in agricultural crops such as corn, wheat, or peanuts, disrupt the normal nucleic acid synthesis, and cause cellular abnormalities, including neoplasms in human liver tissue;[15,16] these represent a few dangerous toxins. Different methods for the detection of toxins were developed, including immunoassays,[17,18] the use of capillary electrokinetic chromatography,[19] and the use of biosensors.[20,21]

The cholera toxin, synthesized by the bacterium *Vibrio cholerae*, is a common contaminant of water or agricultural products irrigated with wastewater. It causes severe dehydration through intestinal fluid loss. The stoichiometry of the six-unit toxin is AB_5 (A, 27 kDa; B, 11.6 kDa). The majority of bacterial exotoxin receptors are carbohydrate components of glycolipids or glycoproteins.[22] Gangliosides are a complex subclass of sphingolipids and are present in the membranes of the human nervous system. They participate in various cellular functions such as cell−cell recognition, interaction with extracellular proteins, and binding of hormones.[23] Many of the gangliosides bind bacterial exotoxins, for example, the GM1 ganglioside (**1**), binds the cholera toxin

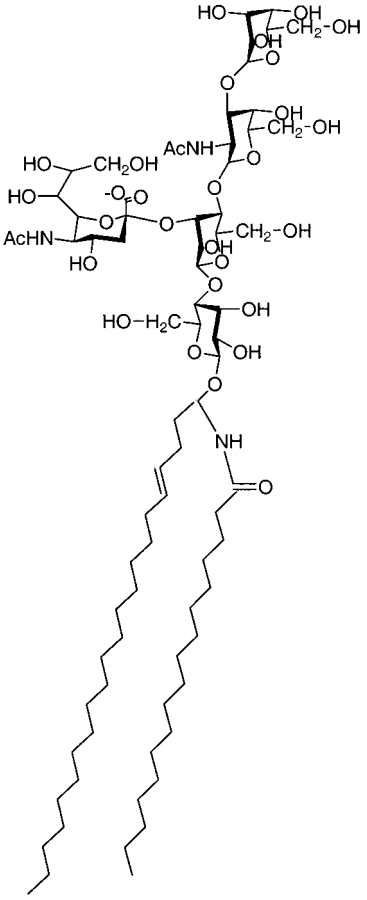

(1) GM1 - monosialoganglioside

(CT).[24] Several studies have used the affinity binding of GM1 to the CT to develop detection schemes for the toxin. The CT could be recognized by GM1-containing supported lipid membranes.[25] Colorimetric detection of the CT was demonstrated with poly(diacetylene)-functionalized liposomes that included GM1,[26] optical sensors for CT that involved resonance energy transfer and self-quenching,[27] and a fluorescence immunoassay for the CT by

(11) Bardea, A.; Katz, E.; Willner, I. *Electroanalysis* **2000**, *12*, 1097−1106.

(12) (a) Patolsky, F.; Katz, E.; Bardea, A.; Willner, I. *Langmuir* **1999**, *15*, 3703−3706. (b) Patolsky, F.; Lichtenstein, A.; Willner, I. *Nat. Biotechnol.* **2000**, *19*, 253−257. (c) Alfonta, L.; Singh, A. K.; Willner, I. *Anal. Chem.* **2001**, *73*, 91−102. (d) Patolsky, F.; Lichtenstein, A.; Kotler, M.; Willner, I. *Angew. Chem., Int. Ed.* **2001**, *40*, 2261−2265.

(13) Monyrvuvvo, V.; Pspini, R.; Dvhisbo, H. In *Sourcebook of Bacterial Protein Toxins*; Alouf, J. E., Freer, J. H., Eds.; Academic Press: New York, 1991; pp 45−56.

(14) Pekala, P. H.; Anderson, B. M. In *The Pyridine Nucleotide Coenzymes*; Everse, J., Anderson, B., You, K.-S., Eds.; Academic Press: New York, 1982; pp 350−355.

(15) Forster, P. L.; Eisenstadt, E.; Miller, J. H. *Proc. Natl. Acad. Sci. U.S.A.* **1983**, *80*, 2615−2698.

(16) Wang, J.-S.; Groopman, J. D. *Mutat. Res.* **1999**, *424*, 167−181.

(17) (a) Pimbly, D. W.; Patel, P. D. *J. Appl. Microbiol.* **1998**, *84* (Suppl.), S98. (b) Wolcott, M. J. In *Immunoassays for Food Poisening Bacterial and Bacterial Toxins*; Waytt, G. M., Ed.; Chapman and Hall: London, 1992.

(18) Singh, A. K.; Harrison, S. H.; Schoeniger, J. S. *Anal. Chem.* **2000**, *72*, 6019−6024.

(19) Wei, J.; Okerberg, E.; Dunlop, J.; Ly, C.; Shear, J. B. *Anal. Chem.* **2000**, *72*, 1360−1363.

(20) (a) Peng, T.; Cheng, Q.; Stevens, R. C. *Anal. Chem.* **2000**, *72*, 1611−1617. (b) Sang, X.; Nolan, J.; Swanson, B. I. *J. Am. Chem. Soc.* **1998**, *120*, 4873.

(21) Rowe-Taitt, C. A.; Cras, J. J.; Patterson, C. H.; Golden, J. P.; Ligler, F. S. *Anal. Biochem.* **2000**, *281*, 123−133.

(22) Fishman, P. H.; Brady, R. O. *Science* **1976**, *194*, 906−915.

(23) (a) Hakomori, S. I. *J. Biol. Chem.* **1990**, *265*, 18713−18716. (b) Fishman, P. H.; Pacuzska, T.; Orlandi, P. A. *Adv. Lipid Res.* **1993**, *25*, 165−187.

(24) van Heyningen, W. E. *Nature* **1974**, *249*, 415−417.

(25) Terrettaz, S.; Stora, T.; Duschl, C.; Vogel, H. *Langmuir* **1993**, *9*, 1361−1369.

(26) (a) Charych, D. H.; Nagy, J. O.; Spevak, W.; Bednarski, M. D. *Science* **1993**, *261*, 585−588. (b) Reicheret, A.; Nagy, J. O.; Spevak, W.; Charych, D. *J. Am. Chem. Soc.* **1995**, *115*, 1146−1147. (c) Charych, D.; Cheng, Q.; Reichert, A.; Kuziemko, G.; Stroh, M.; Nagy, J. O.; Spevak, W.; Stevens, R. C. *Chem. Biol.* **1996**, *3*, 113−120. (d) Pan, J. J.; Charych, D. *Langmuir* **1997**, *13*, 1365−1367.

ganglioside-functionalized liposomes that included fluorescence labels[18] were recently developed.

We report on the development of an ultrasensitive method for the detection of the cholera toxin. We use Faradaic impedance spectroscopy, chronopotentiometry, and quartz crystal microbalance (QCM) measurements as electronic transduction methods. The approach can be further developed for the amplified detection of other toxins.

EXPERIMENTAL SECTION

Chemicals. Horseradish peroxidase (HRP), type VI-A, hydrogen peroxide, 4-chloro-1-naphthol, 3,3′-dithiodipropionic acid-bis-(*N*-hydroxysuccinimide) (DSP) an active ester, protein G, cholera toxin, ganglioside GM1, lipids DSPC (L-distearoylphosphatidylcholine), DMPE (L-dimyristoyl phosphatidylethanolamine), and PA (phosphatidic acid), cholesterol, and other chemicals were from a commercial source (Aldrich or Sigma) and were used as supplied without further purification.

Monoclonal mouse IgG1-anti-B-subunit of cholera toxin was from Biødesign International (Kennebunk, ME).

Ultrapure water from Elgastat (VHQ) source was used throughout this work.

Electrodes Characterization and Pretreatment. Gold wire electrodres (0.5-mm diameter, ~0.2-cm^2 geometrical area, roughness coefficient, ~1.2−1.5) were used for the electrochemical measurements. To remove any previous organic layer, and to regenerate a bare metal surface, the electrodes were treated in a boiling 2 M solution of KOH for 4 h, then rinsed with water, and stored in concentrated sulfuric acid. Immediately before modification, the electrodes were rinsed with water, dried, and soaked for 2 min in fresh piranha solution (30% H_2O_2, 70% H_2SO_4). **Warning:** Piranha solution reacts violently with organic solvents. The resulting electrode was then rinsed with water, soaked for 10 min in concentrated nitric acid, and then rinsed with water once more.

Electrochemical Measurements. A conventional three-electrode cell, consisting of the modified Au electrode, a glassy carbon auxiliary electrode isolated by a glass frit, and a saturated calomel electrode (SCE) connected to the working volume with a Luggin capillary, was used for the electrochemical measurements. The cell was positioned in a grounded Faradaic cage. Impedance and constant-current chronopotentiometry measurements were performed using an electrochemical impedance analyzer (EG&G, model 1025) and potentiostat (EG&G, model 283) connected to a computer (EG&G Software Power Suite 1.03 and 270/250 for impedance and constant-current chronopotentiometry, respectively). All electrochemical measurements were performed in 0.1 M phosphate buffer, pH 7.4, as a background electrolyte solution.

Constant-current chronopotentiometry and Faradaic impedance measurements were performed in the presence of 10 mM $K_3[Fe(CN)_6]/K_4Fe(CN)_6]$ (1:1) mixture, as a redox probe. Impedance measurements were performed at a bias potential of 0.17 V versus SCE using alternating voltage, 10 mV, in the frequency range of 100 mHz to 10 kHz. The impedance spectra were plotted in the form of complex plane diagrams (Nyquist plots). Constant-current chronopotentiometry measurements were performed at a set current of 10 μA and a pulse duration of 10 s. The potential developed at the end of the pulse (after 10 s) was used to derive the electrode resistance.

Microgravimetric Measurements. A QCM analyzer (Fluke 164T multifunction counter, 1.3 GHz, TCXO) linked to a personal computer and a homemade flow cell with a volume of 1.0 mL for the QCM Seiko electrode was employed for the microgravimetric analyses. Quartz crystals (AT-cut, 9 MHz, EG&G) sandwiched between two Au electrodes (area 0.196 cm^2, roughness factor ~3.5) were used.

Electrode Modifications. The electrodes were rinsed with water, dried, and soaked in a 10 mM solution of the DSP-active ester in DMSO for $^1/_2$ h at room temperature. The functionalized electrode was rinsed again in DMSO and water and was incubated in a 100 μg/mL solution of protein G, for 2 h, in buffer solution, room temperature, thus enabling lysines in the protein G to form amide bonds with the active ester attached to the electrode. The protein G-functionalized electrode was then allowed to interact with the Fc fragment of the anti-cholera toxin-antibody, 100 μg/mL, 10 min, room temperature.

Analytical Procedure. The antibody-functionalized electrode interacted with varying concentrations of the cholera toxin for 20 min in phosphate-buffer saline (PBS) solution, 0.1 M, pH 7.4, at room temperature. After attachment of the toxin to the sensing interface, the electrode was incubated in the solution of the GM1-HRP-functionalized liposomes for 20 min at room temperature. 4-Chloro-1-naphthol (**2**) was dissolved initially in ethanol and then the ethanolic stock solution was diluted with 0.1 M phosphate buffer, pH 7.4, to yield the developing solution that included 1×10^{-3} M **2** and 2% (v/v) ethanol. The modified electrodes consisting of the HRP-tagged liposome-functionalized electrodes were incubated for a specified and controlled time intervals in a probe solution consisting of **2**, 1×10^{-3} M, and H_2O_2, 1.5×10^{-4} M. After incubation of the respective electrodes in the probe solution, the electrodes were rinsed with 0.1 M phosphate buffer, pH 7.4, and introduced into the electrochemical cell for the respective analyses (Faradaic impedance spectroscopy or chronopotentiometry). It should be noted that after each step the electrode is rinsed thoroughly with buffer solution, pH 7.4. In the microgravimetric quartz crystal microbalance measurements, the different modification and amplification steps, including the rinsing steps, were performed in a flow cell.

Liposome Preparation. Unilamellar liposomes containing GM1/PA/DMPE/DSPC/cholesterol in molar ratio of 1:1:18:40:40 were prepared by extrusion through polycarbonate membranes as described by Hope et al.[28] Extrusion was carried out using a pneumatic automatic liposome extruder (Liposofast, Avestin, Inc., Vancouver, Canada). The resulting unilamellar liposomes were centrifuged at 3000 rpm for 20 min to remove residual multilamellar vesicles and aggregated lipids. The liposome solution was stored at 4 °C until further use. Liposome preparation and characterization was conducted as previously described by us.[12c] Liposome characteristics were as follows: hydrodynamic diameter, 130.5 ± 12.1 nm; measured ζ potential, −39.5 ± 2.8 mV; number

(27) (a) Song, X. D.; Nolan, J.; Swanson, B. I. *J. Am. Chem. Soc.* **1998**, *120*, 4873−4874. (b) Song, X. D.; Swanson, B. I. *Anal. Chem.* **1999**, *71*, 2097−2107.

(28) Mayer, L. D.; Hope, M. J.; Callis, P. R. *Biochim. Biophys. Acta* **1986**, *858*, 161−168.

Scheme 1. Amplified Sensing of the Cholera Toxin Using a GM1-Tagged HRP-Functionalized Liposome and the Biocatalyzed Precipitation of **3**

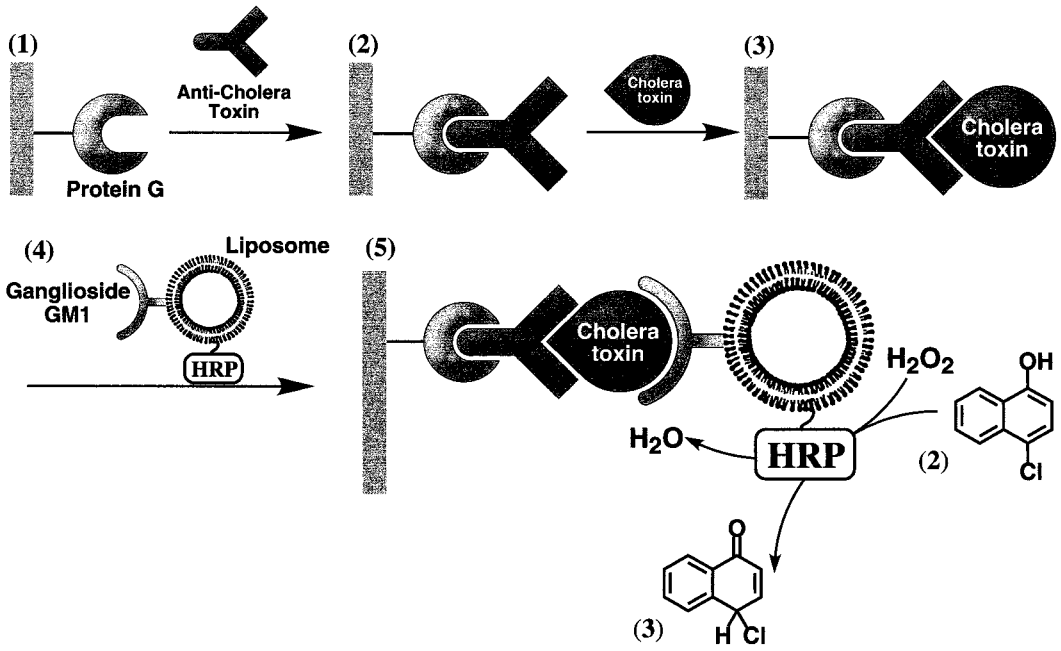

of HRP units per liposome measured to be 40, and the number of receptors (GM1) per liposome, 2280.

RESULTS AND DISCUSSION

Scheme 1 outlines the method that we developed for the amplified detection of the cholera toxin. A protein G monolayer is assembled on an Au support by its covalent attachment to an active ester associated with the electrode. The anti-CT antibody is linked to the protein G interface through its Fc fragment. In the presence of CT in the analyzed sample, the toxin binds to the anti-CT-Ab. Association of the CT with the sensing interface is then amplified by the binding of a ganglioside GM1-functionalized liposome that includes HRP as a biocatalytic label. The HRP-biocatalyzed oxidation of 4-chloro-1-naphthol (**2**) to **3**, in the presence of H_2O_2, yields an insoluble product that precipitates onto the transducer (an Au electrode or an Au/quartz piezoelectric crystal). Note that a single recognition event yields the accumulation of the product **3** on the transducer, thus leading to an amplification path for the detection of CT. The precipitation of the insoluble product on the transducer is anticipated to alter the interfacial properties. Accordingly, Faradaic impedance spectroscopy,[29] constant-current chronopotentiometry,[30] and microgravimetric QCM measurements[31] could act as electronic transduction means for the detection of the CT. In fact, impedance measurements were previously reported as a means to characterize the biocatalyzed deposition of a polymer on an electrode.[32] The alteration of the interfacial properties of the electrode support by the association of the liposomes or upon the precipitation of the insoluble product may be followed by Faradaic impedance spectroscopy and chronopotentiometry.

Impedance spectroscopy is an effective method for probing the features of surface-modified electrodes. The complex impedance can be presented as the sum of the real, $Z_{re}(\omega)$, and imaginary, $Z_{im}(\omega)$, components that originate mainly from the resistance and capacitance of the cell, respectively. Modification of the metallic surface with a biomaterial or an organic layer decreases the double-layer capacitance and retards the interfacial electron-transfer kinetics. The electron-transfer resistance at the electrode is given by eq 1, where R_{Au} and R_{mod} are the electron-

$$R_{et} = R_{Au} + R_{mod} \quad (1)$$

transfer resistance of the unmodified electrode and the variable electron-transfer resistance introduced by the modifier, in the presence of the solubilized redox probe, respectively. A typical shape of a Faradaic impedance spectrum (presented in the form of a Nyquist plot, Z_{im} versus Z_{re} at variable frequencies) includes a semicircle region lying on the Z_{re} axis followed by a straight line. The semicircle portion, observed at higher frequencies, corresponds to the electron-transfer-limited process, whereas the linear part is characteristic for the lower frequencies range and represents the diffusional-limited electron-transfer process. The diameter of the semicircle corresponds to the electron-transfer resistance at the electrode surface, R_{et}. Faradaic impedance spectroscopy is an efficient method to probe and model the interfacial properties of electrodes, yet it suffers from the long

(29) (a) Bard, A. J.; Faulkner, L. R. *Electrochemical Methods. Fundamentals and Applications;* Wiley: New York, 1980. (b) Bond, A. M. *Modern Polarographic Methods in Analytical Chemistry*; Marcel Dekker: New York, 1980. (c) Macdonald, J. R. *Impedance Spectroscopy Emphasizing Solid Materials and Systems*; Wiley: New York, 1987.

(30) (a) Wang, J.; Cai, X. H.; Rivas, G.; Shiraishi, H.; Dontha, N. *Biosens. Bioelectron.* **1997**, *12*, 587−599. (b) Cai, X. H.; Rivas, G.; Farias, P. A. M.; Shiraishi, H.; Wang, J.; Palecek, E. *Anal. Chim. Acta* **1996**, *332*, 49−57.

(31) (a) Buttry, D. A.; Ward, M. D. *Chem. Rev.* **1992**, *92*, 1355−1379. (b) Janshoff, A.; Galla, H.-J.; Steinem, C. *Angew. Chem.* **2000**, *39*, 4004−40032.

(32) Athey, D.; Ball, M.; McNeil, C. J.; Armstrong, R. D. *Electroanalysis* **1995**, *7*, 270−273.

time interval required to record a full spectrum in a broad frequency range. This limitation may be partially resolved by the application of constant-current chronopotentiometry.

Chronopotentiometry is an electrochemical technique that applies a constant current between the working and auxiliary electrodes, while the potential between the working electrode and the reference electrode is altered to retain the desired current value. In the presence of a reversible redox probe in the solution, a Nernstian electrochemical process occurs upon the application of the constant-current value, and the electrode potential is shifted to the characteristic potential of the redox probe in solution. The potential of the electrode is constantly altered according to the R_{ox}/R_{red} ratio of the redox label at the electrode surface. Provided a cathodic current is driven through the solution, after a transition time, τ, the concentration of the oxidized redox species, R_{ox}, at the electrode, drops to zero. Under these conditions, and in the absence of any other redox probe in solution, the potential on the electrode will be sharply shifted to negative values, corresponding to the cathodic discharge of the electrolyte(or the reduction of oxygen) to retain the passage of the desired current value. The association of the liposomes with the electrode surface, and the subsequent biocatalyzed precipitation of an insulating layer on the electrode support, are anticipated to inhibit the interfacial electron-transfer rate constant. Thus, to retain the set current value in the cell, the application of an overpotential, η, on the electrode is required. The overpotential on the electrode, η, will relate to the change in the electrode resistance, R', as a result of modification (formation of the insoluble precipitate) as given by eq 2, where

$$R' = \eta / I = R'_{mod} - R'_{Au} \qquad (2)$$

I is the set constant current and R'_{mod} and R'_{Au} correspond to the resistances of the modified electrode and the bare electrode, respectively. The slope of the $E-t$ curve in the presence of a modifier (or a precipitate) on the electrode is different from the respective curve corresponding to reversible Nernstian behavior of the redox probe since the electron-transfer rate is lower in the presence of the modifier. Thus, for different experiments, the η values should be monitored at identical time intervals of the chronopotentiometric pulse.

The electrode resistance, R', values derived from the chronopotentiometric experiments do not coincide with the electron-transfer resistances, R_{et}, obtained from the Faradaic impedance spectra, and the comparison of these values needs to be made with caution. While the electrode resistances, R', correspond to the entire current flux at the electrode, the electron-transfer resistances, R_{et}, correspond only to the Faradaic current at the electrode interface. Thus, in the chronopotentiometric experiment, the non-Faradaic current originating from the double-layer charging always affects the electrode resistance. At high concentrations of the redox probe ($>10^{-3}$ M), the double-layer charging current is negligible as compared to the Faradaic current. Under these conditions, it is expected that $R' \approx R_{et}$. Furthermore, the double-layer charging current increases with the potential applied onto the electrode. Thus, at high overpotential values, resulting at certain modifications of the electrode, deviations between the total electrode resistances derived from constant-current chronopotentiometry and the electron-transfer resistances determined by Faradaic impedance spectroscopy may be observed, even at high concentrations of the redox probe. In contrast to the Faradaic impedance method, chronopotentiometry measurements are recorded within a few seconds.

The precipitation of the insoluble product on the electrode support can also be probed by microgravimetric QCM analyses.[32] The analysis of the CT according to Scheme 1 includes a sequence of steps that alters the mass on the transducer. The association of the GM1-functionalized liposome induces a mass change on the transducer, and the secondary biocatalyzed precipitation of **3** represents a time-dependent mass change occurring on the transducer.

The frequency change of a quartz crystal, Δf, resulting from a mass alteration on the crystal, Δm, is given by the Sauerbrey relation, eq 3, where f_o is the resonance frequency of the quartz

$$\Delta f = -2f_o^2 \frac{\Delta m}{A(\mu_q \rho_q)^{1/2}} \qquad (3)$$

crystal, A is the piezoelectrically active area, ρ_q is the density of quartz (2.648 g·cm^{-3}), and μ_q is the shear modulus (2.947×10^{11} dyn·cm^{-2} for AT-cut quartz).

Figure 1A exemplifies the buildup of the sensing interface and the analysis of the CT using Faradaic impedance spectroscopy (depicted in the form of Nyquist plots, $Fe(CN)_6^{3-/4-}$ acts as a redox label). The stepwise association of protein G and the anti-CT-Ab results in an increase in the electron-transfer resistances at the electrode surface to 0.5 and 1.9 kΩ, (curves a and b), respectively. This increase in the interfacial electron-transfer resistances is attributed to the partial hydrophobic insulation of the electrode support by the proteins. Parallel microgravimetric QCM analyses indicate that a representative value for the surface coverage of protein G is $\sim 8.8 \times 10^{-11}$ mol·cm^{-2}. Binding of the CT to the anti-CT-Ab further increases the interfacial electron-transfer resistance to 3.5 kΩ (curve c). The association of the HRP-modified ganglioside-functionalized liposomes to the interface increases the interfacial electron-transfer resistance to $\Delta R_{et} = 5.0$ kΩ (Figure 1A, curve d). The subsequent biocatalyzed precipitation of **3** results in a significant increase in the interfacial electron-transfer resistance, $\Delta R_{et} = 14.0$ kΩ. (Figure 1A, curve e), indicating that an amplified detection of the CT is, indeed, observed.

The experimental impedance spectra shown in Figure 1A can be fitted theoretically by the general equivalent circuit shown in the inset of Figure 1A. The solid lines in curves a−e represent the theoretical fits according to this equivalent circuit. It should be noted that each of the steps in the assembly of the sensing interface, in the analysis of the toxin, the association of the HRP-GM1-functionalized liposomes, and the biocatalyzed precipitation of **3**, can be modeled by an electron-transfer resistance element that is in parallel to a capacitance element. The electron-transfer resistance element for an added step corresponds to an electron-transfer resistance that adds in series to the electron-transfer resistances corresponding to the assembly of the units in the previous steps. Similarly, the capacitance element for an added step corresponds to a capacitance element in series with the other capacitance elements corresponding to units assembled in the previous steps.

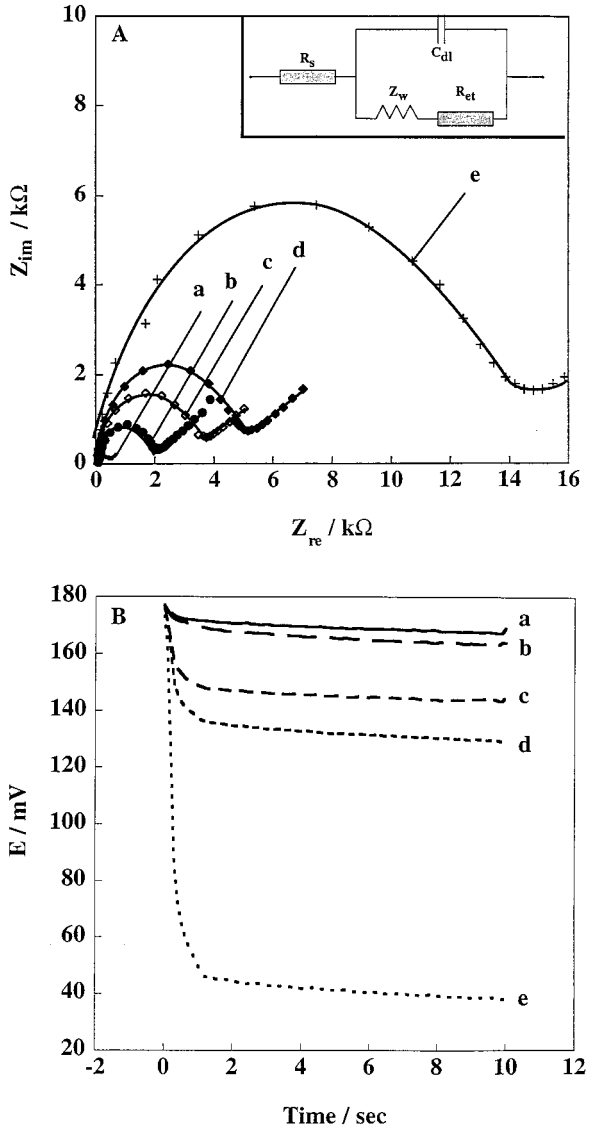

Figure 1. Amplified sensing of the cholera toxin by the biocatalyzed precipitation of **3**, according to Scheme 1, using Faradaic impedance spectroscopy or chronopotentiometry as transduction means. (A) Nyquist plots (Z_{im} vs Z_{re}) for the Faradaic impedance measurements corresponding to the following: (a) the protein G-modified electrode; (b) the protein G-modified electrode treated with the anti-cholera toxin antibody, 100 μg·cm^{-2}, for 10 min; (c) after exposing the sensing interface to the cholera toxin, 1×10^{-13} M, 20 min, room temperature; (d) after further binding of the GM1-HRP-tagged liposomes to the cholera toxin, 1.5×10^{-11} M, 20 min, room temperature; (e) after allowing the biocatalyzed precipitation to occur in the presence of **2**, 1×10^{-3} M, and H_2O_2, 1.5×10^{-4} M, for 10 min. All spectra are recorded in 0.1 M phosphate buffer, pH 7.4, in the presence of 0.01 M $Fe(CN)_6^{3-/4-}$. Solid lines of the Faradaic impedance spectra correspond to the theoretical fitting of the experimental curves according to the equivalent circuit shown in the inset. (B) Transient potential changes upon the application of a chronopotentiometric pulse (constant-current value 10 μA for 10 s) in the presence of 10 mM $[Fe(CN)_6]^{3-/4-}$, curves a−e correspond to the system described in (A).

Similar results are observed upon the analysis of the buildup of the CT-sensing interface and the amplified analysis of the CT using constant-current chronopotentiometry, Figure 1B. The transient-current curves reveal an increase in the overpotentials required to reduce $Fe(CN)_6^{3-}$ upon the assembly of the CT-functionalized liposomes interface (curves a−e). The biocatalyzed precipitation of the insoluble product **3** on the transducer results in a substantial increase in the overpotential (η) required to reduce the redox label (Figure 1B, curve e). The value of the observed overpotential, $\eta = 140$ mV, translates to an electrode resistance that corresponds to $\Delta R = 14.0$ kΩ.

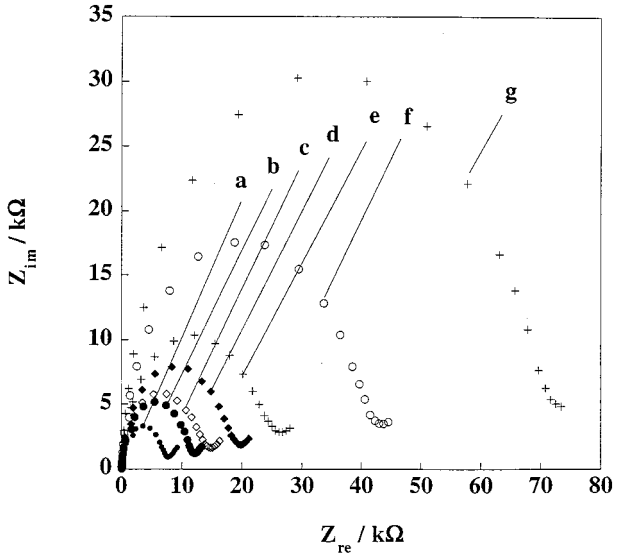

Figure 2. Nyquist plots (Z_{im} vs Z_{re}) corresponding to the Faradaic impedance analysis of the CT, 1×10^{-13} M, by the biocatalyzed precipitation of **3** for different time intervals: (a) 1, (b) 5, (c) 10, (d) 15, (e) 20, (f) 30, and (g) 40 min. The conditions for analyzing CT and the biocatalyzed precipitation are detailed in Figure 1. Data are recorded in phosphate buffer pH 7.4 in the presence of $Fe(CN)_6^{3-/4-}$, 0.01 M.

The extent of amplification is controlled by the time interval used for the biocatalyzed precipitation of **3**. Figure 2 shows the analysis of CT, 1×10^{-13} M, according to Scheme 1, using different time intervals for the precipitation of **3** and Faradaic impedance spectroscopy as transduction means. As the time of precipitation is prolonged, the interfacial electron-transfer resistances increase, indicating the enhanced amplification of the analysis of CT.

Control experiments reveal that all of the components are important for the amplified detection of the CT. Figure 3A shows the Faradaic impedance spectra corresponding to the interaction of the anti-CT-Ab with the HRP-modified GM1-functionalized liposomes and then the result of an attempt to stimulate the biocatalyzed precipitation of **3**. This experiment excludes the interaction of the sensing interface with the CT analyte, and thus, any increase in the interfacial electron-transfer resistance upon the precipitation of **3** may be attributed to the nonspecific binding of the modified liposomes to the anti-CT-Ab sensing interface. Figure 3A, curve c, reveals that the interfacial electron-transfer resistance as a result of nonspecific binding to the sensing interface, is $\Delta R_{et} \cong 2.0$ kΩ. This control experiment defines the noise level of the detection system. Figure 3B shows the results of the second control experiment, where the sensing interface is treated with the CT, 1×10^{-11} M, and the resulting interface is reacted with HRP-modified liposomes that lack the GM1 ganglioside component. An attempt to stimulate the biocatalyzed precipitation of **3** in this system (Figure 3B, curve e) results in an interfacial electron-transfer resistance corresponding to 2.7 kΩ. This latter control experiment reveals the effect of nonspecific

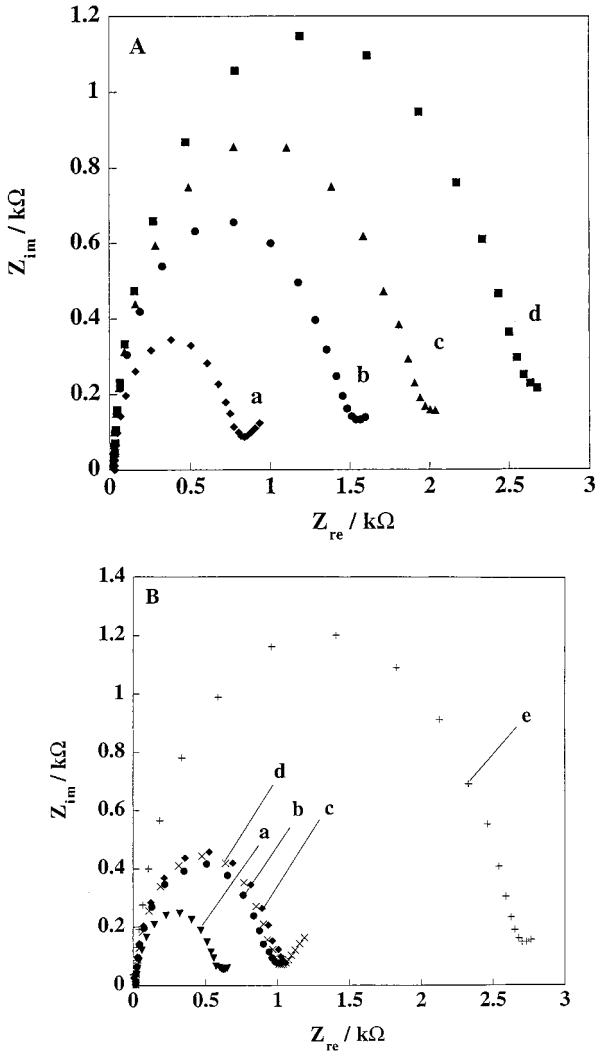

Figure 3. Nyquist plots (Z_{im} vs Z_{re}) corresponding to control experiments related to the analysis scheme of the CT. (A) An attempt to stimulate the biocatalyzed precipitation of **3** on the transducer in the absence of the CT analyte: (a) the spectrum of the protein G-modified electrode; (b) the spectrum after interaction with the anti-CT-antibody, 100 μg·mL^{-1} for 10 min; (c) after incubation of the sensing interface with the GM1-HRP-functionalized liposomes, 1.5 $\times$ 10^{-11} M for 20 min; (d) after an attempt to precipitate **3** in the presence of **2**, 1 $\times$ 10^{-3} M, and H_2O_2, 1.5 $\times$ 10^{-4} M. (B) An attempt to interact the CT/sensing interface affinity complex with HRP-functionalized liposomes that lack the GM1 recognition sites: (a) the spectrum of the protein G-modified electrode; (b) the spectrum after interaction with the anti-CT-antibody, 100 μg·mL^{-1} for 10 min; (c) after incubation of the sensing electrode with the CT, 1 $\times$ 10^{-11} M, for 20 min; (d) after interaction of the resulting electrode with the HRP-functionalized liposomes, 1.5 $\times$ 10^{-11} M, for 20 min; (e) after an attempt to stimulate the biocatalyzed precipitation of **3** in the presence of **2**, 1 $\times$ 10^{-3} M, and H_2O_2, 1.5 $\times$ 10^{-4} M. All impedance measurements were recorded in 0.1 M phosphate buffer, pH 7.4 in the presence of $Fe(CN)_6^{3-/4-}$, 0.01 M.

binding of the liposome to the CT-modified interface. We realize that, for the amplified detection of the CT, it is mandatory to bind the HRP-modified liposomes to the toxin by the specific CT-GM1-ganglioside affinity interactions. Similarly, a control experiment where the protein G-modified electrode, which lacks the anti-CT-Ab, was treated with the CT and then with the GM1-functionalized-HRP liposomes, followed by an attempt to stimulate the biocatalyzed precipitation of **3**, results in a change of the interfacial electron-transfer resistance from ΔR_{et} = 0.8 kΩ for the protein G-functionalized electrode to $\Delta R_{et} \approx$ 2.2 kΩ for the electrode resulting upon the attempt to precipitate **3**. These control experiments correspond to the effect of nonspecific adsorption of the CT to the protein G interface, and it reveals the functions of the anti-CT-Ab in the analysis of the CT.

The method can be applied for the quantitative analysis of the CT. Figure 4A shows the Faradaic impedance spectra (Nyquist plots) corresponding to the biocatalyzed precipitation of **3** by four different electrodes that sense different concentrations of the CT. Figure 4B shows the current transients observed upon constant-current chronopotentiometry analyses of the CT by the same electrodes. It is evident that the electron-transfer resistances increase as the concentration of CT in the analyzed samples is higher. This is consistent with the fact that higher concentrations of the CT increase the binding of the GM1-HRP liposome labels that stimulate the biocatalyzed precipitation of **3**. Figure 4C shows the calibration curves corresponding to the changes in the electron-transfer resistance, ΔR_{et}, or electrode resistances, $\Delta R'$, upon the analysis of the CT by the biocatalyzed precipitation of **3**. It is evident that the CT can be easily analyzed with a sensitivity limit of 1 $\times$ 10^{-13} and a S/N = 7.

We believe that our analysis scheme reveals significantly improved sensitivities as compared to previous methods. Colorimetric detection of the CT revealed[26d] a sensitivity limit of ~1 $\times$ 10^{-6} M, whereas fluoroimmunoassay suggested the detection of the CT with a detection limit of ~5 $\times$ 10^{-8} M. Thus, our method reveals a 10^4-fold sensitivity improvement in the analysis of the toxin.

QCM experiments enable the microgravimetric transduction of the amplified detection of CT by the biocatalyzed precipitation of **3**. Curves a and b of Figure 5 show the time-dependent frequency changes of the anti-CT-Ab-functionalized Au/quartz crystals that sense the CT at concentrations that correspond to 2 $\times$ 10^{-8} and 1.2 $\times$ 10^{-12} M, respectively. Addition of the anti-CT-Ab to the protein G-functionalized Au/quartz crystals (Figure 5, point B) results in a frequency decrease of ~220 Hz. At point B, the sensing interfaces are interacted with the CT at the different concentrations. Upon treatment of the sensing interface with the CT, 2 $\times$ 10^{-8} M, a minute frequency change of ~−10 Hz is noticed, whereas treatment of the modified crystal with CT, 1.2 $\times$ 10^{-12} M, does not lead to any noticeable change in the crystal frequencies. Thus, the direct microgravimetric detection of the CT by the sensing interface is impossible in the concentration range of 2 $\times$ 10^{-8}−1.2 $\times$ 10^{-12} M, using quartz crystal microbalance measurements. Using the frequency change of −10 Hz, resulting upon the binding of CT (2 $\times$ 10^{-8} M) to the sensing interface, we estimate the surface coverage of the toxin at this bulk concentration to be 4.4 $\times$ 10^{-13} mol·cm^{-2}. Treatment of the resulting interfaces with the GM1-functionalized-HRP-liposomes (point D, Figure 5) results in, for both systems, a time-dependent frequency decrease indicating the association of the liposomes to the CT units. The high molecular weight of the liposome micromembrane units enables their microgravimetric detection although the surface coverage of the base CT units is low and undetectable. Thus, the GM1-functionalized liposomes provide a primary amplification label for the detection of CT. As the

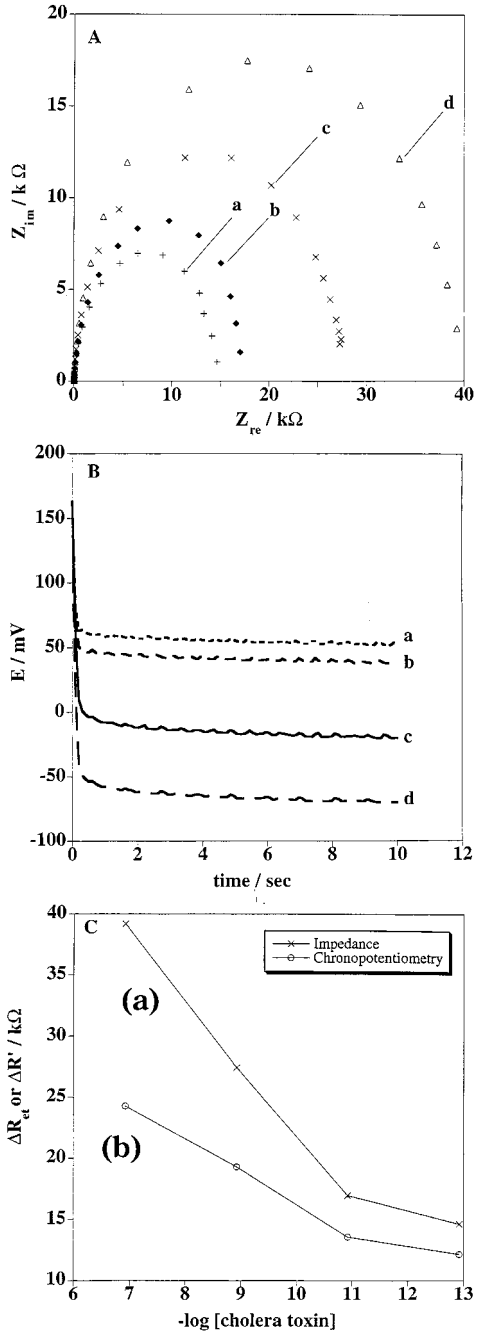

Figure 4. (A) Faradaic impedance spectra corresponding to the amplified analysis of different concentrations of the CT by the biocatalyzed precipitation of **3**: (a) 1×10^{-13}, (b) 1×10^{-11}, (c) 1×10^{-9}, and (d) 1×10^{-7} M CT. The stepwise processes to analyze the CT and to precipitate **3** are detailed in the caption of Figure 1. (B) Transient potential changes upon the analysis of different concentrations of CT by the biocatalyzed precipitation of **3**: (a) 1×10^{-13}, (b) 1×10^{-11}, (c) 1×10^{-9}, and (d) 1×10^{-7} M CT. Transients are recorded in 0.1 M phosphate buffer, pH 7.2, which includes $Fe(CN)_6^{3-/4-}$, 0.01 M. A chronopotentiometric pulse that maintains a constant current of 100 μA for 10 s is applied on the electrode. The experimental details for the stepwise assembly of the electrodes are detailed in the caption of Figure 1. (C) Calibration curves corresponding to the changes in the electron-transfer resistance at the electrode, ΔR_{et} (a) or the eletrode resistances, ΔR (b), upon the amplified sensing of different concentrations of the CT. ΔR_{et} or $\Delta R'$ corresponds to the difference in the electron-transfer resistance (or electrode resistance) after the biocatalyzed preicpitation of **3** and the electron-transfer resistance (or electrode resistance) of the modified electrode prior to the biocatalyzed precipitation of **3**.

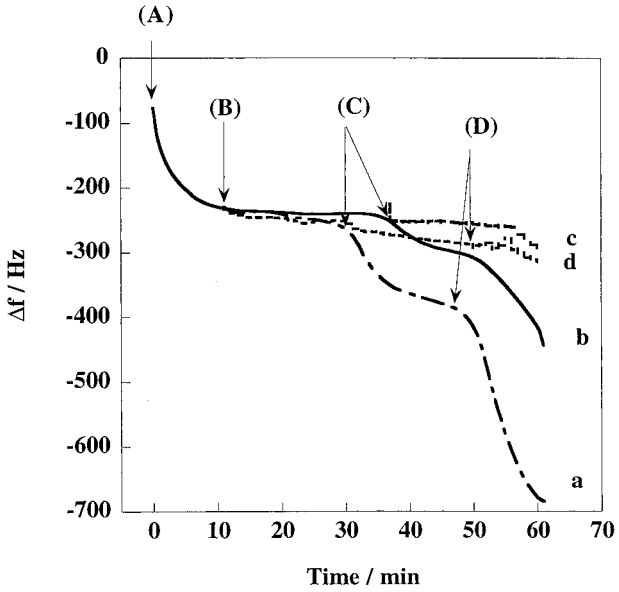

Figure 5. Time-dependent frequency changes of the functionalized Au/quartz crystal (9 MHz) after the following: (a) amplified analysis of the CT, 2×10^{-8} M, according to Scheme 1; (b) amplified analysis of the CT, 1.2×10^{-12} M according to Scheme 1.;(c) a control experiment that challenges the sensing interface with the labeled liposomes and the biocatalyzed precipitation of **3**, without treatment of the sensing interface with the CT; (d) a control experiment that analyzes the CT, 1×10^{-9} M, in the presence of the HRP-functionalized liposomes that lack the GM1 recognition sites. The experimental numbered points correspond to the following: (A) treatment of the protein G-functionalized crystal with anti-CT-Ab, 100 $\mu g \cdot mL^{-1}$; (B) treatment of the sensing interfaces with the respective concentrations of CT as detailed in (a), (b), and (d); (C) treatment of the modified surfaces with the GM1/HRP functionalized liposomes, for systems a−c and with the HRP-modified liposomes for system d. (D) The biocatalyzed precipitation of **3** in the presence of **2**, 1×10^{-3} M, H_2O_2, 1.5×10^{-4} M.

concentration of the CT analyte increases, the frequency changes as a result of the binding of the biocatalytic liposomes are higher, implying an elevated content of the liposomes on the sensing interface. The increase in the content of the biocatalytic label on the sensing interface at higher bulk concentrations of the CT is reflected nicely upon the precipitation of **3** on the Au/quartz crystal (Figure 5, point D). As the bulk concentration of CT is higher, the biocatalyzed precipitation of **3** is enhanced. For example, at concentrations of 2×10^{-8} and 1.2×10^{-12} M CT, the biocatalyzed precipitation of **3** for 10 min results in frequency changes of $\Delta f = -340$ Hz and $\Delta f = -140$ Hz, respectively, which translate to a mass increase on the crystal of 1.3 and 0.6 $\mu g \cdot cm^{-2}$, respectively. It is interesting to note absolute values and the shapes of the time-dependent frequency changes upon the biocatalyzed precipitation of **3**. Very significant frequency changes (hundreds of hertz) are observed, and the frequency values decrease constantly without reaching any saturation value. These results demonstrate nicely the "active amplification" of the CT detection by the biocatalyzed precipitation of **3**. Curves c and d of Figure 5 show the frequency changes of the crystal upon performing the appropriate control experiments. Figure 5, curve c, shows the interaction of the anti-CT-Ab interface that was not treated with the CT, with the HRP-modified GM1-functionalized liposomes and the attempt to perform the secondary biocatalyzed

precipitation of **3**. A minute frequency change of $\Delta f = -35$ Hz is observed that originates from the nonspecific binding of the labeled liposomes to the sensing interface, resulting in a low amount of precipitate on the transducer. Figure 5, curve d, shows the time-dependent frequency changes of the Au/quartz crystal resulting upon the sensing of the CT by the anti-CT-Ab interface followed by the treatment of the assembly with HRP-modified liposomes, which lack GM1, and the attempt to stimulate the secondary biocatalyzed precipitation of **3**. A minute change in the crystal frequency is observed upon the attempt to precipitate **3**, $\Delta f = -23$ Hz. This frequency change originates from the nonspecific binding of the HRP-functionalized liposomes to the sensing interface. The latter control experiment indicates the importance of the specific CT-ganglioside GM1 affinity interactions in the amplified detection scheme of the toxin. It should be noted that the two control experiments reveal that the nonspecific adsorption of the biocatalytic-liposome-amplifying label results in a frequency change of ~30 Hz, which may be considered as the noise level of the system. Thus, the analysis of the CT at the concentration of 1.2×10^{-12} M is detected with a S/N of ~6.

CONCLUSIONS

The present study employed enzyme-modified (HRP)-ganglioside (GM1)-functionalized liposomes as a biocatalytic affinity label for the amplified electronic transduction of cholera toxin detection. The biocatalytic affinity label binds to an antibody/toxin complex, and the biocatalyzed precipitation of an insoluble product on the respective transducers enables the amplification of the sensing event. The method allows the sensitive detection of the CT with an unprecedented detection limit of 1.0×10^{-13} M. The liposomes used in the present study function only as a carrier unit for the GM1 ganglioside and the biocatalytic amplifier. By the incorporation of other gangliosides in the liposomes, the development of biocatalytic affinity labels for other toxins may be envisaged. The different electronic transduction means used in the present study to follow the formation of the insoluble product on the electronic transducers, i.e., Faradaic impedance spectroscopy, constant-current chronopotentiometry, and quartz crystal microbalance measurements, provide general tools to follow the sensing events of the toxin.

ACKNOWLEDGMENT

The study is supported by the Israel Ministry of Science as an Infrastructure Project on Biomicroelectronics. L.A. acknowledges a Levi Eshkol fellowship, the Israel Ministry of Science. Sandia National laboratories is a multiprogram laboratory operated by Sandia Corporation, a Lockheed Martin Company, for the United States Department of Energy under contract DE-AC04-94AL85000.

Received for review May 9, 2001. Accepted July 24, 2001.

AC010542E